Holstein model in infinite dimensions

J. K. Freericks
Institute for Theoretical Physics and Department of Physics, University of California, Santa Barbara, California 93106-4030

M. Jarrell
Department of Physics, University of Cincinnati, Cincinnati, Ohio 45221

D. J. Scalapino
Institute for Theoretical Physics and Department of Physics, University of California, Santa Barbara, California 93106-4030

(Received 18 January 1993; revised manuscript received 27 May 1993)

Monte Carlo simulations are performed to examine superconductivity and charge-density-wave fluctuations in the infinite-dimensional electron-phonon Holstein model. The electron-phonon system interpolates between an attractive, static, Falicov-Kimball model that always exhibits charge-density-wave order and an attractive, instantaneous, Hubbard model that always superconducts as a function of phonon frequency. The maximum charge-density-wave transition temperature at half-filling is an order of magnitude smaller than the effective electronic bandwidth and is virtually independent of the phonon frequency. The maximum superconducting transition temperature depends strongly on phonon frequency and is bounded from above by the maximum charge-density-wave transition temperature. The exact solution is compared to both weak-coupling expansions and strong-coupling expansions. The effective phonon potential becomes anharmonic and develops a double-well structure that deepens as the electron-phonon interaction increases.

I. INTRODUCTION

The interaction between fermionic degrees of freedom (conduction electrons in a solid) and bosonic degrees of freedom (harmonic phonons of a lattice) is known as the electron-phonon problem and is still not fully understood for all values of the parameters. Migdal[1] and Eliashberg[2] pioneered the study of the electron-phonon problem in the limit where the phonon energy scale is much smaller than the electronic energy scale. In this limit, vertex corrections may be neglected (Migdal's theorem[1]) and a self-consistent theory can be constructed that describes both superconductivity and charge-density-wave-Peierls order. Migdal-Eliashberg theory (ME) predicts that the transition temperature in the superconducting (SC) channel will increase without an upper bound[3] as the electron-phonon interaction strength increases. A strong-coupling expansion, however, predicts that the system has a transition temperature that vanishes as the electron-phonon interaction strength increases and that the charge-density-wave (CDW) channel is favored over the SC channel.[4] As a result, one would like to know if there is a maximum transition temperature, what parameters set the scale for this transition temperature, and what is the character of the ordered state? In order to answer such questions one needs exact solutions and reliable approximation techniques that are unbiased toward SC or CDW order.

Monte Carlo (MC) simulations allow one to bridge the gap between weak-coupling and strong-coupling expansions. Previous work has concentrated on one-dimension[5] where it was found that the system always dimerized into a CDW-Peierls state at half-filling, and on two dimensions[6–9] where it was found that the CDW state was unstable with respect to filling and the system superconducted when doped sufficiently far away from half-filling. Here we will explore the Holstein model[10] in infinite dimensions.

In the Holstein[10] Hamiltonian chosen, the conduction electrons interact with local phonon modes:

$$H=-\frac{t^*}{2\sqrt{d}}\sum_{\langle j,k\rangle\sigma}(c_{j\sigma}^{\dagger}c_{k\sigma}+c_{k\sigma}^{\dagger}c_{j\sigma})+\sum_j(gx_j-\mu)(n_{j\uparrow}+n_{j\downarrow})+\frac{1}{2}M\Omega^2\sum_j x_j^2+\frac{1}{2M}\sum_j p_j^2\,, \tag{1}$$

where $c_{j\sigma}^{\dagger}$ ($c_{j\sigma}$) creates (destroys) an electron at site j with spin σ, $n_{j\sigma}=c_{j\sigma}^{\dagger}c_{j\sigma}$ is the electron number operator, and x_j (p_j) is the phonon coordinate (momentum) at site j. The hopping matrix elements span the nearest neighbors of a hypercubic lattice in d dimensions and the rescaled matrix element t^* sets the energy scale (all energies are measured in units of t^*). The localized bosonic degree of freedom has a mass M and a frequency Ω associated with it; the combination $\kappa\equiv M\Omega^2$ is the spring constant that measures the stored energy per unit length squared in the boson field. The electron-phonon coupling constant g is an energy per unit length and determines the strength of the electron-phonon interaction. A useful combination of fundamental parameters is the bipolaron binding energy

$$U\equiv-\frac{g^2}{M\Omega^2}=-\frac{g^2}{\kappa}\,, \tag{2}$$

0163-1829/93/48(9)/6302(13)/$06.00

which determines the energy scale for the effective electron-electron interaction mediated by the bosonic field. Once the energy scale is set by t^*, there are three additional parameters in the Holstein model: the electron-phonon coupling strength g; the phonon mass M; and the spring constant κ. Only two of these three parameters are free to vary. One can choose to set a length scale by fixing the spring constant and then allow the mass and coupling strength to vary. Instead, we have chosen to fix the mass ($M=1$) and have selected $|U|$ and Ω as the free parameters. The limit $\Omega\rightarrow\infty$ is equivalent to $M\rightarrow 0$ and the limit $\Omega\rightarrow 0$ is equivalent to $M\rightarrow\infty$, while the limits $|U|\rightarrow 0$ and $|U|\rightarrow\infty$ are equivalent to $g\rightarrow 0$ and $g\rightarrow\infty$, respectively. The chemical potential is denoted μ and the particle-hole symmetric point (half-filled band) corresponds to $\mu=U$.

The Holstein Hamiltonian describes the interaction of fermionic degrees of freedom with bosonic degrees of freedom that can be phonons, excitons, plasmons, etc., so that the frequency Ω is not necessarily much smaller than the electronic energy scale t^*. The Holstein model corresponds to the following idealizations of electron-phonon systems in real materials: (1) the electrons only hop between nearest neighbors in a single band; (2) the phonons have no dispersion (Einstein modes); (3) the phonons are harmonic; (4) the phonons do not modify the hopping integral. Assumptions (1) and (2) are the simplest and most natural ones to make in the limit of large spatial dimensions—the effect of hopping between next-nearest neighbors frustrates the system and is more difficult to incorporate, while the bosonic density of states becomes very sharply peaked at the maximum phonon frequency as $d\rightarrow\infty$. Assumption (3) is easy to modify within a MC framework, but is difficult to model using approximation techniques. As will be seen below, the effective bosonic potential becomes anharmonic (with a double-well structure) even when one starts with a harmonic potential. Assumption (4) may also be modified. In this case one is describing a different type of electron-phonon system with a Hamiltonian of the Su-Schrieffer-Heeger type,[11] where the phonon coordinate couples to the electrons through a dynamic hopping integral $t^*(x)$.

In this contribution the electron-phonon problem is examined in the limit of infinite spatial dimensions ($d\rightarrow\infty$). Section II describes how the system is mapped onto a self-consistent (local) impurity problem in the limit of infinite spatial dimension. Section II also includes a discussion of the limits where the phonon energy scale is much larger than the electronic energy scale (instantaneous limit), where the phonon energy scale is much smaller than the electronic energy scale (static limit), and how the Holstein model interpolates between these two. The different approximation methods for both weak and strong coupling are reviewed in Sec. III and compared with the MC simulations. Conclusions are presented in Sec. IV.

II. THE INFINITE-DIMENSIONAL LIMIT

In infinite dimensions ($d\rightarrow\infty$) the hopping from one lattice site to its nearest neighbor is scaled to zero [see Eq. (1)]. Naively one might expect that all of the physical properties become local (and trivial) in this limit. However, the hopping integral is scaled to zero in such a fashion that the free-electron kinetic energy remains finite while the self-energy for the single-particle Green's function and the irreducible vertex functions have no momentum dependence and are functionals of the local Green's function.[12–14] The many-body problem is solved by mapping it onto an auxiliary impurity problem[15,16] in a time-dependent field (that mimics the hopping of an electron onto a site at time τ and off the site at a time τ'). The action for the impurity problem is found by integrating out all of the degrees of freedom of the other lattice sites in a path-integral formalism.[17] The result is an effective action

$$\begin{aligned} S_{\rm eff}=&\sum_\sigma\int_0^\beta d\tau\int_0^\beta d\tau' c_\sigma^\dagger(\tau)G_0^{-1}(\tau-\tau')c_\sigma(\tau') \\ &+\sum_\sigma\int_0^\beta d\tau[gx(\tau)-\mu]c_\sigma^\dagger(\tau)c_\sigma(\tau) \\ &+\frac{1}{2}M\int_0^\beta d\tau[\Omega^2x^2(\tau)+\dot{x}^2(\tau)]\ , \end{aligned} \tag{3}$$

where G_0^{-1} is the "bare" Green's function that contains *all of the dynamical information of the other sites of the lattice.* The interacting Green's function is determined by

$$G_n^{-1}\equiv G^{-1}(i\omega_n)=G_0^{-1}(i\omega_n)-\Sigma(i\omega_n)\ , \tag{4}$$

at each Matsubara frequency $\omega_n=(2n+1)\pi T$. The self-consistency relation that maps the impurity problem onto the infinite-dimensional lattice equates the full Green's function for the impurity problem with the local Green's function for the lattice

$$\begin{aligned} G_{jj}(i\omega_n)&=\sum_{\mathbf{k}}G(\mathbf{k},i\omega_n) \\ &=\sum_{\mathbf{k}}[i\omega_n+\mu-E(\mathbf{k})-\Sigma(i\omega_n)]^{-1}\ , \\ &\equiv F_\infty[i\omega_n+\mu-\Sigma(i\omega_n)]\ , \end{aligned} \tag{5}$$

with $F_\infty(z)$ the scaled complimentary error function of a complex argument[17]

$$\begin{aligned} F_\infty(z)&=\frac{1}{\sqrt{\pi}}\int_{-\infty}^{\infty}dy\ \frac{\exp(-y^2)}{z-y} \\ &=-i\ \mathrm{sgn}[\mathrm{Im}(z)]\sqrt{\pi}e^{-z^2}\mathrm{erfc}\{-i\ \mathrm{sgn}[\mathrm{Im}(z)]z\}\ . \end{aligned} \tag{6}$$

The dynamics of the (local) impurity problem is identical to the dynamics of the Anderson impurity model[13,15–18] and may be solved by using the quantum MC algorithm of Hirsch and Fye[19] [this latter point is easiest to see by integrating out the electronic degrees of freedom which enter quadratically in the effective action (3) and is identical to the numerical procedures used to solve the infinite-dimensional Hubbard model[18,20–22]]. It is important to note that since one does not *a priori* know the bare Green's function G_0^{-1} in Eq. (3), one must iterate the

MC algorithm to determine a self-consistent solution for the Green's function of the infinite-dimensional lattice. The procedure[18] is to begin with a bare Green's function G_0^{-1} (typically the noninteracting Green's function is chosen for the starting point), use the quantum MC algorithm to determine the self-energy Σ, calculate the lattice Green's function from Eq. (5), and determine a new bare Green's function from Eq. (4). This process is iterated until convergence is reached (typically 7–9 iterations are sufficient).

A variety of two-particle properties may also be calculated in the quantum MC approach[23] since the irreducible vertex function is also local. The static susceptibility for CDW order is given by

$$\chi^{\mathrm{CDW}}(\mathbf{q}) \equiv \frac{T}{2N} \sum_{\mathbf{R}_j-\mathbf{R}_k\sigma\sigma'} e^{i\mathbf{q}\cdot(\mathbf{R}_j-\mathbf{R}_k)} \int_0^\beta d\tau \int_0^\beta d\tau' [\langle T_\tau n_{j\sigma}(\tau) n_{k\sigma'}(\tau')\rangle - \langle n_{j\sigma}(\tau)\rangle\langle n_{k\sigma'}(\tau')\rangle]$$

$$\equiv T \sum_{mn} \tilde{\chi}^{\mathrm{CDW}}(\mathbf{q}, i\omega_m, i\omega_n) = T \sum_{mn} \tilde{\chi}^{\mathrm{CDW}}_{mn}(\mathbf{q}) , \tag{7}$$

at each ordering wave vector $\mathbf{q}$. Dyson's equation for the two-particle Green's function becomes[18,23]

$$\tilde{\chi}^{\mathrm{CDW}}_{mn}(\mathbf{q}) = \tilde{\chi}^0_m(\mathbf{q})\delta_{mn} - T \sum_p \tilde{\chi}^0_m(\mathbf{q}) \Gamma^{\mathrm{CDW}}_{mp} \tilde{\chi}^{\mathrm{CDW}}_{pn}(\mathbf{q}) , \tag{8}$$

with $\Gamma^{\mathrm{CDW}}_{mn}$ the (local) irreducible vertex function in the CDW channel.

The noninteracting CDW susceptibility $\tilde{\chi}^0_n(\mathbf{q})$ in Eq. (8) is defined in terms of the single-particle Green's function

$$\tilde{\chi}^0_n(\mathbf{q}) \equiv -\frac{1}{N} \sum_{\mathbf{k}} G_n(\mathbf{k}) G_n(\mathbf{k}+\mathbf{q})$$

$$= -\frac{1}{\sqrt{\pi}} \frac{1}{\sqrt{1-X^2(\mathbf{q})}} \int_{-\infty}^{\infty} dy \, \frac{e^{-y^2}}{i\omega_n + \mu - \Sigma_n - y} F_\infty \left[\frac{i\omega_n + \mu - \Sigma_n - X(\mathbf{q}) y}{\sqrt{1-X^2(\mathbf{q})}} \right] \tag{9}$$

and all of the wave-vector dependence is included in the scalar[15,24]

$$X(\mathbf{q}) \equiv \frac{1}{d} \sum_{j=1}^{d} \cos \mathbf{q}_j .$$

The mapping $\mathbf{q} \rightarrow X(\mathbf{q})$ is a many-to-one mapping that determines an equivalence class of wave vectors in the Brillouin zone. "General" wave vectors are all mapped to $X=0$ since $\cos\mathbf{q}_j$ can be thought of as a random number between -1 and 1 for "general" points in the Brillouin zone. Furthermore, all possible values of X ($-1 \le X \le 1$) can be labeled by a wave vector that lies on the diagonal of the first Brillouin zone extending from the zone center ($X=1$) to the zone corner ($X=-1$). There are three values of X where the integral for $\tilde{\chi}^0_n(X)$ in Eq. (9) can be performed analytically[15]: $X=-1$; $X=0$; and $X=1$. The results are

$$\tilde{\chi}^0_n(X=-1) = -\frac{G_n}{i\omega_n + \mu - \Sigma_n} ; \quad \tilde{\chi}^0_n(X=0) = -G_n^2 ;$$
$$\tilde{\chi}^0_n(X=1) = 2[1 - (i\omega_n + \mu - \Sigma_n) G_n] ; \tag{10}$$

at these three special points.

The irreducible vertex function $\Gamma^{\mathrm{CDW}}_{mn}$ may be calculated in the quantum MC procedure by solving the local equation

$$\tilde{\chi}^{\mathrm{CDW}}_{mn}(\mathrm{local}) = -G_m^2 \delta_{mn} + T \sum_p G_m^2 \Gamma^{\mathrm{CDW}}_{mp} \tilde{\chi}^{\mathrm{CDW}}_{pn}(\mathrm{local}) , \tag{11}$$

with the local CDW susceptibility defined by the following two-particle Green's function

$$\tilde{\chi}^{\mathrm{CDW}}_{mn}(\mathrm{local}) \equiv -\frac{1}{2} T^2 \sum_{\sigma\sigma'} \int_0^\beta d\tau_1 \cdots d\tau_4 e^{-i\omega_m(\tau_4-\tau_3)} e^{-i\omega_n(\tau_2-\tau_1)}$$

$$\times [\langle T_\tau c^\dagger_\sigma(\tau_4) c_\sigma(\tau_3) c^\dagger_{\sigma'}(\tau_2) c_{\sigma'}(\tau_1)\rangle - \langle c^\dagger_\sigma(\tau_4) c_\sigma(\tau_3)\rangle \langle c^\dagger_{\sigma'}(\tau_2) c_{\sigma'}(\tau_1)\rangle] . \tag{12}$$

A similar procedure is used for the singlet s-wave SC channel. The corresponding definitions are as follows: The static susceptibility in the superconducting channel is defined to be

$$\chi^{\mathrm{SC}}(\mathbf{q}) \equiv \frac{T}{N} \sum_{\mathbf{R}_j - \mathbf{R}_k} e^{i\mathbf{q}\cdot(\mathbf{R}_j - \mathbf{R}_k)} \int_0^\beta d\tau \int_0^\beta d\tau' \langle T_\tau c_{j\uparrow}(\tau) c_{j\downarrow}(\tau) c^\dagger_{k\downarrow}(\tau') c^\dagger_{k\uparrow}(\tau') \rangle$$

$$\equiv T \sum_{mn} \tilde{\chi}^{\mathrm{SC}}(\mathbf{q}, i\omega_m, i\omega_n) = T \sum_{mn} \tilde{\chi}^{\mathrm{SC}}_{mn}(\mathbf{q}) \tag{13}$$

for superconducting pairs that carry momentum $\mathbf{q}$; Dyson's equation becomes

$$\tilde{\chi}^{\mathrm{SC}}_{mn}(\mathbf{q}) = \tilde{\chi}^{0\prime}_m(\mathbf{q}) \delta_{mn} - T \sum_p \tilde{\chi}^{0\prime}_m(\mathbf{q}) \Gamma^{\mathrm{SC}}_{mp} \tilde{\chi}^{\mathrm{SC}}_{pn}(\mathbf{q}) , \tag{14}$$

with $\Gamma^{\mathrm{SC}}_{mn}$ the corresponding irreducible vertex function for the SC channel; the noninteracting pair-field susceptibility becomes

$$\tilde{\chi}^{0\prime}_n(\mathbf{q}) \equiv \frac{1}{N} \sum_{\mathbf{k}} G_n(\mathbf{k}) G_{-n-1}(-\mathbf{k}+\mathbf{q})$$

$$= \frac{1}{\sqrt{\pi}} \frac{1}{\sqrt{1-X^2(\mathbf{q})}} \int_{-\infty}^{\infty} dy \, \frac{e^{-y^2}}{i\omega_n + \mu - \Sigma_n - y} F_\infty \left[\frac{i\omega_{-n-1} + \mu - \Sigma_{-n-1} - X(\mathbf{q}) y}{\sqrt{1-X^2(\mathbf{q})}} \right] \tag{15}$$

with the special value

$$\chi^{0\prime}_n(X=1) = G_n / (i\omega_{-n-1} + \mu - \Sigma_{-n-1})$$

for the SC pair that carries no net momentum; and finally the irreducible vertex function is determined by solving the local equation

$$\tilde{\chi}^{\mathrm{SC}}_{mn}(\mathrm{local}) = |G_m|^2 \delta_{mn} - T \sum_p |G_m|^2 \Gamma^{\mathrm{SC}}_{mp} \tilde{\chi}^{\mathrm{SC}}_{pn}(\mathrm{local}) , \tag{16}$$

with the local SC susceptibility defined by the following two-particle Green's function

$$\tilde{\chi}^{\mathrm{SC}}_{mn}(\mathrm{local}) = -T^2 \int_0^\beta d\tau_1 \cdots d\tau_4 e^{-i\omega_m(\tau_4 - \tau_3)} e^{-i\omega_n(\tau_2 - \tau_1)} \times \langle T_\tau c_\uparrow(\tau_4) c_\downarrow(\tau_3) c^\dagger_\downarrow(\tau_2) c^\dagger_\uparrow(\tau_1) \rangle . \tag{17}$$

The single- and two-particle Green's functions G, χ^{CDW}, and χ^{SC} are all calculated using quantum MC methods. The imaginary-time interval from 0 to β is discretized into L times slices of equal width $\Delta\tau = \beta/L$ and the grand-canonical MC scheme is used to evaluate the relevant path integrals (using the quantum MC algorithm of Hirsch and Fye[19]). Both local moves, in which the phonon coordinate is shifted by a different amount at each time slice, and global moves, in which the phonon coordinate was shifted by a uniform amount for every time slice, were incorporated in the MC algorithm.[8] The values of L used ranged from 20 to 160 with the largest values of $\Delta\tau$ reserved for the lowest temperatures. Calculation at half-filling were performed for values of $\Delta\tau = 0.2$ and 0.4 and then scaled toward $\Delta\tau \to 0$ to try to remove the lowest-order Trotter error which is estimated to be proportional to $\Delta\tau^2$. Calculations off of half-filling were performed at the fixed value $\Delta\tau = 0.4$ since lower temperatures were needed to find the SC instability (it was found that the Trotter error for these values of $\Delta\tau$ was similar to the statistical error). No sign problem was found at any filling.

It is instructive to compare the MC simulations to the limiting behavior of the Holstein model. In particular, the limits when the phonon frequency Ω is much larger than or much smaller than the electronic energy scale t^* are examined. To begin, the bosonic degrees of freedom in the effective action (3) are integrated out to produce a purely electronic action with a time-dependent effective electron-electron interaction.[25] This effective electron-electron interaction is expressed in terms of the bare phonon propagator

$$U_{\mathrm{eff}}(\tau) = g^2 D_0(\tau) . \tag{18}$$

In the limit $\Omega \to \infty$, the phonon reacts instantaneously to the electronic motion, and the effective electron-electron interaction becomes nonretarded $U_{\mathrm{eff}}(\tau) \to U\delta(\tau)$. In this case the Holstein model maps onto an attractive Hubbard model[26] with electron-electron interaction strength U. The attractive Hubbard model is known to be superconducting for all electronic fillings.[27] An additional SU(2) pseudospin symmetry[28] exists at half-filling that requires CDW order to coexist with SC order. This is the so-called supersolid phase.

In the static limit in which $\Omega \to 0$, the phonon coordinate does not change in time and the effective electron-electron interaction becomes constant $U_{\mathrm{eff}}(\tau) \to U$. The conduction electrons interact with a localized (continuous) degree of freedom that possesses no dynamics (and enters only through annealed thermodynamic averages). This many-body problem is identical to the system described by the attractive Falicov-Kimball model[29] in the large S limit (a continuous number of static configurations) with spin-$\frac{1}{2}$ conduction electrons. In the large U limit the mapping simplifies to a two-state version (spinless Falicov-Kimball model) which has already been solved in the infinite-dimensional limit[15,30] (Aubry, Abramovici, and Raimbault discuss the strong-coupling

limit using rigorous perturbative arguments[31]). The details of the mapping onto the Falicov-Kimball model are described in the Appendix. It is known that the Falicov-Kimball model orders in a CDW state because the phonon field is static and does not support a superconducting instability.[31,32]

The Holstein model interpolates between these two limits as a function of the phonon frequency Ω. Therefore, we expect CDW order to be favored for small values of Ω and electron concentrations near half-filling; SC order should be favored for large values of Ω and away from half-filling. The infinite-dimensional results for the transition temperature to CDW order at half-filling for the Hubbard model,[18,20–22] for the Falicov-Kimball model[15] (see the Appendix for details), and for the Holstein model at the intermediate value $\Omega/t^*=0.5$ are compared in Fig. 1. The horizontal axis measures the interaction strength from $U=0$ to $-\infty$. The vertical axis plots the transition temperature in units of t^*. Note that the maximum CDW transition temperature is on the order of $0.15t^*$ and appears to be virtually independent of the phonon frequency, i.e., there is no enhancement of the maximum CDW transition temperature for intermediate values of the phonon frequency. The position of the peak shifts from the point $U/t^*=-0.92$ (Falicov-Kimball model, $\Omega\to 0$), to the point $U/t^*=-1.56$ (Holstein model, $\Omega/t^*=0.5$), and finally to the point $U/t^*=-3.0$ (Hubbard model, $\Omega\to\infty$). Furthermore, in the small $|U|$ regime, the Falicov-Kimball model provides an upper bound to the CDW transition temperature for the Holstein model and the Hubbard model provides a lower bound. This situation is reversed in the large $|U|$ limit with the Falicov-Kimball model providing the lower bound and the Hubbard model providing the upper bound to the CDW transition temperature of the Holstein model.

For a fixed value of U the transition temperature to the commensurate CDW state ($X=-1$) at half-filling is expected to be the largest transition temperature (to either CDW or SC order) as a function of electron filling because of the enhancement provided by Fermi surface nesting (the hypercubic lattice in d dimensions is bipartite). This implies that the maximum transition temperature for the electron-phonon system is determined solely by the electronic bandwidth, is virtually independent of phonon frequency, and occurs in the CDW channel.

As the system is doped away from half-filling one expects there to be a competition between commensurate CDW order (at the "antiferromagnetic" point $X=-1$), incommensurate CDW order (ordering at values of X intermediate between 1 and -1), phase separation of electrons and holes (CDW ordering at the "ferromagnetic" point $X=1$), and superconductivity. The MC simulations only found evidence for ordering in the commensurate CDW state ($X=-1$) and in the zero-momentum SC paired state ($X=1$) for all values of the parameters tested. The CDW-ordered state remains "locked" at the "antiferromagnetic" point for a very wide range of dopings away from half-filling. This behavior appears to be

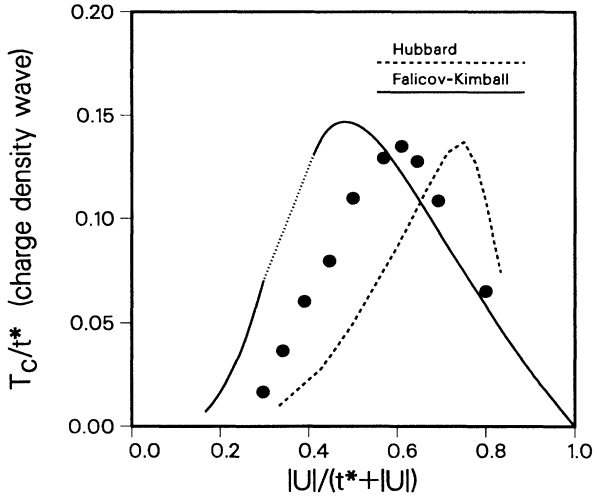

FIG. 1. Comparison of the transition temperature T_c to the commensurate charge-density-wave state ($X=-1$) for the Holstein model at different phonon frequencies Ω. The dashed line is the $\Omega\to\infty$ limit (Hubbard model), the solid line is the $\Omega\to 0$ limit (Falicov-Kimball model), and the solid dots are the Monte Carlo results from $\Omega/t^*=0.5$. The horizontal axis measures the effective electron-electron interaction strength $|U|$ from 0 to ∞ and the vertical axis measures the transition temperature. The dotted line is a linear interpolation that connects the transition temperature curves from weak-coupling and strong-coupling expansions in the static limit (see the Appendix for details). The maximum T_c is always on the order of $0.15t^*$ and occurs at a value of U that shifts from $-0.92t^*$ at low frequencies to $-3.0t^*$ at high frequencies.

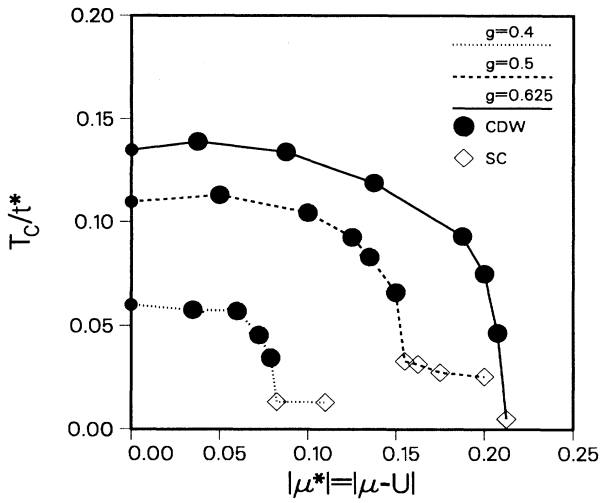

FIG. 2. Transition temperatures in the Holstein model for $\Omega/t^*=0.5$ as a function of the reduced chemical potential $|\mu^*|=|\mu-U|$. The horizontal axis plots μ^* and the vertical axis plots T_c/t^*. Three values of g are shown: $g=0.4t^*$ (dotted line); $g=0.5t^*$ (dashed line); and $g=0.625t^*$ (solid line). The solid dots represent commensurate CDW order at $X=-1$ and the open diamonds represent SC order with zero-momentum pairs ($X=1$). The SC transition temperatures increases to $0.03t^*$ ($g=0.5$) and then rapidly decreases (the SC transition temperature at $g=0.625$ is less than $0.01t^*$ and may be exponentially small).

different from what was found in two dimensions[6–9] where the system rapidly changed from CDW order to SC order as a function of doping. However, the effective value of u/t^* in the two-dimensional work[6–9] is on the order of -0.7 which is in the weak-coupling regime ($g \approx 0.4$ in the present units). The transition from CDW to SC is quite rapid with respect to doping in this regime (see the next section). Figure 2 displays the results for the transition temperature of the doped Holstein model with $\Omega/t^*=0.5$ at three different values of the electron-phonon coupling ($g=0.4$, 0.5, and 0.625). The solid dots denote CDW order and the open diamonds denote SC order. The transition temperature is plotted as a function of the reduced chemical potential $\mu^*=\mu-U$ that measures the absolute shift of the chemical potential away from the particle-hole symmetric point ($\mu^*=0$). The SC transition temperature is too low to be accurately determined at the largest coupling strength ($g=0.625$), however, once the chemical potential becomes large enough there is no CDW instability and the SC susceptibility increases as T is lowered which indicates a transition will take place at a low enough temperature. An upper bound for the SC transition temperature at $g=0.625$ is $T_c < 0.01t^*$, but exponentially small values cannot be ruled out. Note that the calculations away from half-filling were performed at a fixed value of $\Delta\tau=0.4$ while those at half-filling were scaled to $\Delta\tau \to 0$. One can see that the Trotter error at $\Delta\tau=0.4$ is similar to the statistical errors in these cases.[33]

III. APPROXIMATION METHODS

In this section different approximation techniques for both weak ($|U| \ll t^*$) and strong ($|U| \gg t^*$) coupling are reviewed and compared to the MC results to determine the regions of their validity. The approximation techniques are applied directly to the impurity model. The mapping onto the infinite-dimensional lattice employs the same iterative procedure used in the MC simulations (see Sec. II for details).

The lowest-order weak-coupling expansions determine the self-energy by a self-consistent perturbation theory. The most common approximations are Migdal-Eliashberg (ME) theory[1,2] or conserving Hartree-Fock (CHF) theory.[25] Both of these approximations will be described below.

The ME theory neglects all vertex corrections [which enter to order Ω/t^* and vanish in the static limit ($\Omega \to 0$)] and is expected to be inaccurate for large phonon frequencies. The CHF approximation is a conserving approximation in the sense of Baym and Kadanoff[34] in that the conservation laws for momentum, energy, and particle number are preserved to all orders in the approximation. Conserving approximations[25,34] are derived by beginning with an expression for the free energy in terms of skeleton diagrams of the self-consistent Green's function G. The self-energy is determined by functional differentiation of the free energy with respect to the Green's function. Susceptibilities are calculated by adding an external field and differentiating the corresponding operator average with respect to the perturbing field in the limit where the field approaches zero.

The electronic self-energy is determined[35] by [see Fig. 3(a)]

$$\Sigma_n = -g^2 T \sum_m D_{n-m} G_m \ , \tag{19}$$

with the phonon propagator given by

$$D_l \equiv D(i\omega_l) = -\frac{1}{M(\Omega^2+\omega_l^2)+\Pi_l} \ ; \quad \omega_l = 2\pi l T \ . \tag{20}$$

Here $\Pi_l \equiv \Pi(i\omega_l)$ is the phonon self-energy. The full Green's function G is determined self-consistently from the self-energy Σ and the bare Green's function G_0 by the procedure outlined in Sec. II. The self-consistent solution for the self-energy is iterated until the maximum deviation for one element of the set $\{\Sigma_n\}$ is less than one part in 10^8. The energy cutoff was set to include 256 positive Matsubara frequencies.

In the unrenormalized ME approximation and the CHF approximation the phonon self-energy Π_l is neglected. In what is called the renormalized ME approximation,[7] Π_l is approximated by [see Fig. 3(b)]

$$\Pi_l = 2g^2 T \sum_n G_{l+n} G_n \ . \tag{21}$$

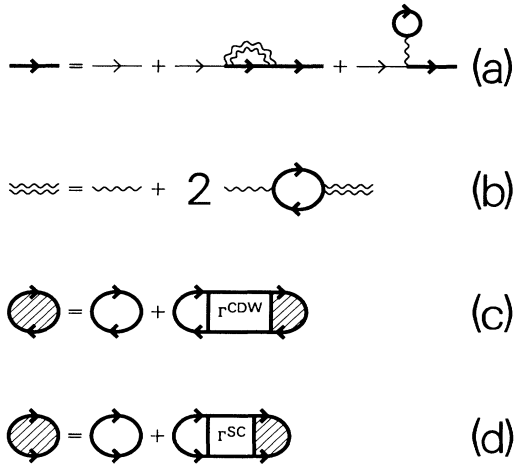

FIG. 3. Feynman diagrams for the Holstein model. Solid lines denote electron propagators (bold lines are the full Green's function G, light lines are the bare Green's function G_0), wiggly lines denote phonon propagators (double lines denote the full phonon propagator, single lines denote the bare phonon propagator). Dyson's equation for the electronic Green's function is given in (a) and includes both Hartree and Fock terms (the Hartree terms are independent of frequency and can be absorbed into a renormalized chemical potential μ). The full phonon propagator is renormalized as in (b) for the renormalized ME theory (the factor of 2 arises from a sum over spins), but is equal to the bare phonon propagator for both the unrenormalized ME theory and the CHF theory. The CDW susceptibility is represented schematically in (c) with the irreducible vertex function Γ^{CDW} given by Eqs. (22) or (23). The SC susceptibility is represented schematically in (d) with the irreducible vertex function Γ^{SC} given by Eq. (24).

Here the electron propagators are self-consistently calculated from Eqs. (19) and (20).

The susceptibilities for CDW and SC order are given by Eq. (8) and Eq. (14), respectively [see Figs. 3(c) and 3(d)]. Both unrenormalized and renormalized ME theories neglect vertex corrections. The irreducible vertex function for the CDW channel becomes

$$\Gamma_{mn}^{\mathrm{CDW}}(\mathrm{ME})=2U\ , \tag{22}$$

and is independent of frequency. In the CHF approximation[25] the irreducible vertex function for the CDW channel becomes

$$\Gamma_{mn}^{\mathrm{CDW}}(\mathrm{CHF})=2g^2D_0-g^2D_{m-n}$$
$$=U\left[2-\frac{\Omega^2}{\Omega^2+\omega_{m-n}^2}\right]\ , \tag{23}$$

including both direct and exchange contributions. The irreducible vertex function for the SC channel becomes

$$\Gamma_{mn}^{\mathrm{SC}}=g^2D_{m-n}=U\left[1+\frac{\omega_{m-n}^2}{\Omega^2}+\frac{\Pi_{m-n}}{M\Omega^2}\right]^{-1}\ , \tag{24}$$

for both ME theories and the CHF theory (note $\Pi_{m-n}=0$ for the unrenormalized ME theory and for the CHF theory).

The ME approximation neglects the exchange diagrams in the CDW channel and will produce the wrong behavior in the high-phonon-frequency limit ($\Omega\to\infty$). The CHF approximation, on the other hand, incorporates the exchange diagrams which produce an effective interaction Γ^{CDW} that interpolates between the low-frequency limit $\Gamma^{\mathrm{CDW}}\to 2U$ and the high-frequency limit $\Gamma^{\mathrm{CDW}}\to U$.

As the transition temperature (to a CDW-ordered state or a SC-ordered state) is approached from above, the susceptibility (in the relevant channel) diverges. Therefore, one can determine the transition temperature by finding the temperature where the scattering matrix (in the relevant channel)

$$T_{mn}=T\chi_m^0\Gamma_{mn} \tag{25}$$

has unit eigenvalue.[36]

The results for the three different approximation schemes are compared to the MC results in Fig. 4 for an intermediate value of the phonon frequency ($\Omega/t^*=0.5$). The transition temperature to the commensurate ($X=-1$) CDW state at half-filling is plotted as a function of the electron-phonon coupling strength g. The unrenormalized ME approximation is plotted as a dotted line, the renormalized ME approximation as a solid line, and the CHF approximation as a dashed line. One can see that the CHF approximation is similar to the unrenormalized ME approximation but has a more accurate value of the effective electron-electron interaction. The renormalized ME theory displays the correct qualitative behavior of developing a peak in $T_c(g)$. However, the equations become unstable to an iterative solution at a value of $g\approx 0.67t^*$, and both the peak position and peak height are underestimated.

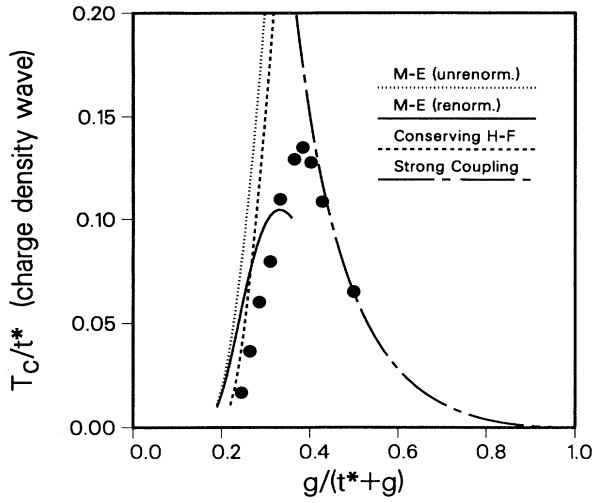

FIG. 4. Comparison of the approximation methods with the MC results for the commensurate CDW transition at half-filling in the Holstein model with $\Omega/t^*=0.5$. The horizontal axis plots the electron-phonon coupling strength from weak coupling $g\to 0$ to strong coupling $g\to\infty$, and the vertical axis records the transition temperature in units of t^*. The unrenormalized Migdal-Eliashberg (ME) theory (dotted line), the renormalized ME theory (solid line), conserving Hartree-Fock (CHF) approximation (dashed line), and strong-coupling theory (chain-dashed line) are compared to the MC results (solid dots). The CHF approximation is more accurate at small g because it properly takes into account the contribution from exchange diagrams in Γ^{CDW}. The renormalized ME approximation displays the correct qualitative behavior of developing a peak but the equations become unstable as g increases.

These results suggest that a conserving fluctuation-exchange[25] approximation which renormalizes the phonon propagator and treats CDW and SC fluctuations on the same footing may produce more accurate results. The conserving fluctuation-exchange approximation is more difficult to perform because one must self-consistently solve an integral equation for the irreducible vertex functions (that now depend on three Matsubara frequencies).

In the opposite limit of strong coupling ($|U|\gg t^*$), the electrons interact so strongly that they pair into bipolarons and the Holstein Hamiltonian can be mapped onto an anisotropic Heisenberg antiferromagnet in a uniform external field. It is easiest to see this by performing a canonical transformation of the Holstein model and restricting the Hilbert space to consist of only empty sites and paired sites. The technique is similar to the Schrieffer-Wolff transformation[37] as applied to the Hubbard model.[38] The phonon can be "integrated out" by calculating the effects (through second order) of the hopping. The bipolaron fluctuates via virtual processes where one electron hops onto a neighboring site and either the remaining electron hops to the same neighboring site (producing an effective hopping of the bipolaron) or the original electron hops back to the original site (producing an effective bipolaron-bipolaron interaction).[39]

One must take into account the Frank-Condon factors for the overlap between harmonic-oscillator states that are centered about different positions (the origin for the harmonic oscillator when zero, one, or two electrons are on a site is 0, $-g/M\Omega^2$, or $-2g/M\Omega^2$, respectively). The end result is

$$H=2U\sum_j\left[(J_j^z)^2-\frac{1}{4}\right]-2(\mu-U)\sum_j J_j^z + \sum_{\langle jk\rangle}\left[j_\perp\frac{1}{2}(J_j^+J_k^-+J_j^+J_k^-)+j_\parallel\left[J_j^zJ_k^z-\frac{1}{4}\right]\right], \quad (26)$$

where the pseudospin operators $\mathbf{J}_j$ are defined by[28]

$$J_j^+=(-1)^j c_{j\uparrow}^\dagger c_{j\downarrow}^\dagger\ ,\quad J_j^-=(J_j^+)^\dagger\ , \qquad J_j^z=\tfrac{1}{2}(n_{j\uparrow}+n_{j\downarrow}-1)\ , \quad (27)$$

and the factor $(-1)^j$ is 1 for the A sublattice and (-1) for the B sublattice of the hypercubic lattice in d dimensions. The transformed Hamiltonian is an anisotropic (XXZ) Heisenberg antiferromagnet (spin $\frac{1}{2}$) in an external magnetic field [$h=2(\mu-U)=2\mu^*$].

If it is assumed that the temperature is much smaller than the phonon frequency Ω, then the harmonic oscillator lies in its ground state when there are no electrons or two electrons on a site. In this case, it is easy to determine the exchange parameters $j_\parallel(j_\perp)$ parallel (perpendicular) to the z axis.[5] The result is

$$j_\parallel=\frac{|t^*|^2}{d|U|}\left[1+\sum_{n=1}^{\infty}\frac{(-S)^n}{(1+S)(2+S)\cdots(n+S)}\right], \quad (28)$$

$$j_\perp=\frac{|t^*|^2}{d|U|}e^{-2S}\left[1+\sum_{n=1}^{\infty}\frac{(S)^n}{(1+S)(2+S)\cdots(n+S)}\right], \quad (29)$$

where the polaron band-narrowing parameter S is defined to be $S\equiv|U|/\Omega$.

It is easy to establish that $j_\parallel$ is always larger than $j_\perp$ with equality occurring only in the limit $S\to 0$. Furthermore, in the limit $S\to\infty$, $j_\perp\to 0$ exponentially fast and $j_\parallel\to|t^*|^2/2d|U|$. Therefore, the system always orders in the CDW phase if the phonon frequency is finite and the electron-phonon coupling is large enough.

The correspondence between the magnetization of the pseudospin operators and CDW or SC order is easily made by examination of Eq. (27). When the staggered magnetization orders along the z axis it signifies a CDW ordered state at the commensurate ($X=-1$) point. When the staggered magnetization orders along the x axis it corresponds to SC ($X=1$). The external magnetic field is twice the reduced chemical potential (zero field corresponds to half-filling).

In infinite dimensions the mean-field theory for the spin-$\frac{1}{2}$ anisotropic Heisenberg antiferromagnetic is exact.[4] The transition temperature to the CDW ($X=-1$) state is[4]

$$T_c(\mathrm{CDW})=\tfrac{1}{2}\rho_e(2-\rho_e)j_\parallel d\ , \quad (30)$$

where ρ_e is the electron concentration, and the transition temperature for the SC state is[4]

$$T_c(\mathrm{SC})=\frac{(\rho_e-1)j_\perp d}{\ln[\rho_e/(2-\rho_e)]}\ . \quad (31)$$

In the limit $S\to\infty$ the transition temperature to the SC state approaches zero and the transition temperature to the CDW state approaches $\rho_e(2-\rho_e)/4|U|$ which is identical to the behavior of a spinless Falicov-Kimball model (in the strong-coupling limit) with $U_{\mathrm{FK}}=2U$.

The transition temperature from the strong-coupling expansion is plotted as a chain-dashed line in Fig. 4. The MC data agree extremely well with the strong-coupling expansion for all points to the right of the peak in the transition temperature curve. The strong-coupling expansion appears to be valid over a much wider range than the weak-coupling expansion.

In order to shed some light on the transition from weak to strong coupling the MC simulations were sampled to determine a time-averaged effective phonon potential. The probability $P(x)$ that the phonon coordinate $x(\tau_l)$ lies in the interval from x to $x+\delta x$ was calculated for each time slice τ_l and averaged over all time slices. If all correlations along the τ axis are ignored, an effective phonon potential $V_{\mathrm{eff}}(x)$ can then be extracted from the probability distribution[40]

$$P(x)\equiv c\exp[-\beta V_{\mathrm{eff}}(x)]\ , \quad (32)$$

as a function of temperature (c is an overall normalization constant). This effective phonon potential should *qualitatively* describe the important physics in the Holstein model.

When the electron-phonon coupling is weak, the effective phonon potential is expected to be harmonic and centered at the single-electron equilibrium coordinate $x_1=-g/M\Omega^2$. As the coupling increases, a double-well structure should develop with minima located at the equilibrium coordinates for zero ($x_0=0$) and two ($x_2=-2g/M\Omega^2$) electrons. The effective potential $V_{\mathrm{eff}}(x^*)$ is plotted versus the rescaled coordinate $x^*=-M\Omega^2x/2g$ in Fig. 5 for four different values of the electron-phonon coupling strength ($g=0.325$, 0.5, 0.625, and 1.0) at a temperature $T=\frac{1}{7}$. Note that the potential $V_{\mathrm{eff}}(x^*)$ is symmetric about $x^*=0.5$ at half-filling and the normalization constant c in Eq. (32) has been chosen so that $V_{\mathrm{eff}}(x^*=0.5)=0$.

In the case of weak coupling ($g=0.325$) one can see the potential appears harmonic. The potential flattens when $U\approx t^*$ ($g=0.5$) and a double-well structure develops. The barrier height appears to grow linearly with g as does the separation of the minima. The peak of the $T_c(g)$ curve for the CDW transition (see Fig. 4) is reached at the point where the barrier height is on the order of T_c ($g=0.625$). Beyond this point ($g=1.0$) the lattice displacement coordinate becomes trapped in one of two minima and T_c decreases.

These results are qualitatively similar to those found by Yu and Anderson[41] in their work on the $A15$ compounds. They differ in the dependence of the barrier

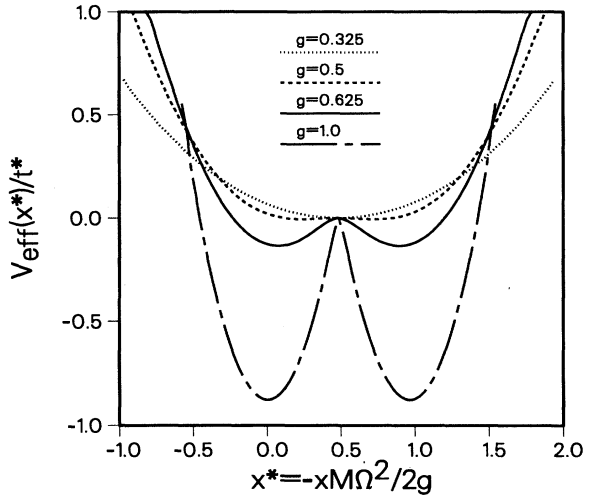

FIG. 5. Effective phonon potential for the Holstein model at half-filling with $\Omega/t^*=0.5$ and $\beta=7$. The horizontal axis measures the renormalized coordinate $x^*=-xM\Omega^2/2g$ and the vertical axis measures $V_{\rm eff}$ in units of t^*. The effective potential is plotted for four values of g: $g=0.325$ (dotted line); $g=0.5$ (dashed line); $g=0.625$ (solid line); and $g=1.0$ (chain-dashed line). The effective phonon potential is symmetric about $x^*=0.5$. Note that the effective phonon potential appears harmonic for small g, becomes flat at $g=0.5$, and develops a double-well structure that deepens as g increases. The peak of the T_c curve at half-filling (see Fig. 4) occurs when the barrier height is on the order of T_c.

height and the separation of the minima on the coupling strength g (a linear dependence is found here while the barrier height increases logarithmically and the separation of the minima saturates in Ref. 41).

Finally, the question of what is the phase diagram for the Holstein model as a function of the phonon frequency Ω is addressed. It is known that as $\Omega\rightarrow 0$ the ground state is always a CDW, whereas in the limit $\Omega\rightarrow\infty$ the ground state is always a SC. How does the electron-phonon system change its behavior from a static CDW ordered system to a SC? This question is partially answered by calculating the phase diagram in the weak-coupling approach (CHF) and in the strong-coupling approach and comparing the results to MC simulations. Note that the weak-coupling approximation should be accurate when the transition region occurs at small values of $|U|$ and the strong-coupling approximation should be accurate when the transition region occurs at large values of $|U|$. The grand-canonical formalism with a fixed chemical potential is used in order to compare the approximation methods to the MC results.

In the weak-coupling approach (CHF approximation), the transition temperature for a CDW at an ordering vector characterized by the scalar X can be calculated for all values of $-1\leq X\leq 1$. Ordering at $X=-1$ corresponds to the commensurate two-sublattice CDW (the "antiferromagnetic" point), ordering at $-1<X<1$ corresponds (in general) to an incommensurate CDW, and ordering at $X=1$ corresponds to phase separation of the electrons and the holes (the "ferromagnetic" point). The transition temperature for the SC phase can also be calculated. The SC transition temperature is always a maximum for the state composed of zero-momentum pairs ($X=1$). The transition temperatures are calculated for a fixed value of the reduced chemical potential μ^* and the critical chemical potential is determined where the CDW transitions disappears. It turns out that the transition temperature has a discontinuous jump

$$[T_c(\text{CDW})\neq T_c(\text{SC})]$$

at this critical chemical potential in the CHF approximation. This implies that the electron concentration at T_c will also be discontinuous in the CHF approximation at the boundary between CDW and SC order. The schematic "phase diagram" that plots $\rho_e(T_c)$ versus the coupling strength g is presented in Fig. 6 for the phonon frequency $\Omega/t^*=0.5$. This "phase diagram" is the simplest approximation to a zero-temperature phase diagram

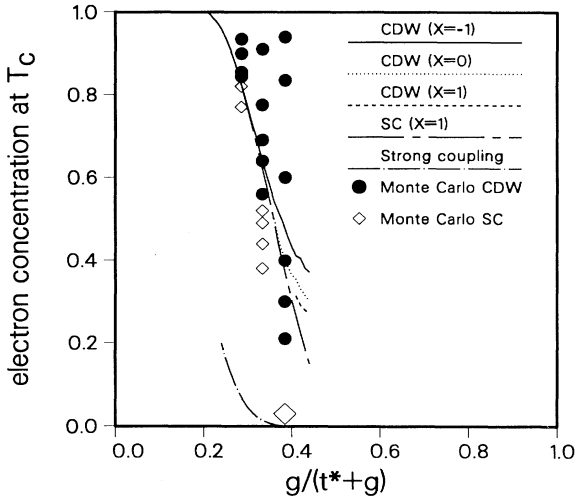

FIG. 6. Schematic zero-temperature "phase diagram" for the Holstein model at $\Omega/t^*=0.5$. The electron-phonon coupling strength is plotted on the horizontal axis and the electron concentration at T_c is plotted on the vertical axis. The MC results are depicted by solid dots (commensurate CDW order) and open diamonds (SC order) at three values of g. The solid line is the CHF approximation for ρ_e at the critical chemical potential where the system no longer orders in a CDW at $X=-1$. The dotted (dashed) lines are the similar results for the CDW at $X=0$ ($X=1$). The region between the solid and dashed line is the region where the CHF approximation predicts incommensurate CDW order. The chain-dashed line is the electron concentration at the SC transition temperature at the critical chemical potential where the system no longer has any CDW order. The chain-dotted line is the strong-coupling expansion (ρ_e is continuous at T_c in the strong-coupling approximation). Note that the CHF approximation is very accurate at $g=0.4$ but rapidly loses accuracy as g increases (the MC simulation found no evidence for incommensurate CDW order). Note also that the strong-coupling approximation deteriorates very rapidly as g decreases below 0.75.

that can be made within a formalism that is restricted to the homogeneous (high-temperature) phase. It should represent the zero-temperature phase diagram if the temperature dependence of the electron concentration can be neglected from $T=0$ to T_c. The solid line represents $\rho_e(T_c)$ at the critical chemical potential where the transition to the commensurate CDW at $X=-1$ disappears. The dotted line (dashed line) is the corresponding electron concentration for the critical CDW transition at $X=0$ ($X=1$). (The region between the solid line and the dashed line is the region where the CDW orders at an incommensurate wave vector.) The chain-dashed line represents the $\rho_e(T_c)$ for the zero-momentum SC state at the critical chemical potential (where the last CDW instability disappears). It is expected that the phase boundary separating CDW and SC order will not be discontinuous in a canonical formalism (where the chemical potential is adjusted as a function of temperature to keep the electron concentration at a fixed value) and will lie between the SC line and the lowest CDW line in Fig. 6. The CHF approximation becomes inaccurate for large values of g.

The results from a MC simulation are presented as closed dots and open diamonds in Fig. 6 for three values of g ($g=0.4$, 0.5, and 0.625). The closed dots represent transitions to a CDW state at $X=-1$ and the open diamonds represent transitions to the SC state. The CHF approximation appears to be quite accurate for the smallest value of g. The MC data showed no evidence for any incommensurate CDW order or for phase separation.

Note that the maximum SC transition temperature found in the CHF approximation was on the order of $0.03t^*$ (at $g=0.67$) which is a factor of 5 smaller than the maximum CDW transition temperature and agrees with the maximum temperature seen in the MC simulations (at $g=0.5$). This implies that the maximum SC transition temperature is very strongly dependent on the phonon frequency, and is significantly smaller than $0.15t^*$ in the small-phonon-frequency limit.

A strong-coupling expansion does not display any discontinuity in the electron concentration at T_c. The transition line from CDW to SC is found by equating the two transition temperatures in Eqs. (30) and (31). The critical electron concentration $\rho_e(T_c)$ is then easily determined as a function of g. The result for the strong-coupling expansion is given by the chain-dotted line in Fig. 6. One can see that it does not agree with the CHF approximation or the MC data. At first, it might appear surprising that the strong-coupling expansion is so accurate for the CDW properties at half-filling (see Fig. 4) but appears to describe the SC properties quite poorly. This paradox is resolved by realizing that the transition region from CDW to SC behavior is occurring at small to moderate values of g and low electron densities, where the strong-coupling expansion is not expected to be very accurate (the strong-coupling expansion predicts a transition from CDW to SC behavior occurs at $S\approx 1$ which is outside of the strong-coupling regime for $\Omega/t^*=0.5$).

It is clear that the transition from CDW order to SC order occurs when the electron-electron interaction strength $|U|$ is the same order of magnitude as the phonon frequency Ω. The phase boundary is a nearly vertical line in the ρ_e-g plane. A weak-coupling approximation is expected to be much more accurate than a strong-coupling approximation in determining the position of this phase boundary when the phonon frequency is smaller than the electronic energy scale. The opposite should occur when the phonon frequency is larger than the electronic energy scale. If incommensurate CDW order exists, it is present in only a very restricted range of phase space; the MC simulations found no evidence for incommensurate behavior at any filling or interaction strength. Finally, it should be noted that the work in two dimensions[6–9] appears to agree quite well with the infinite-dimensional work. The two-dimensional work is in the weak-coupling regime ($g\approx 0.4$) where the transition from CDW to SC order occurs quite rapidly as a function of doping. No evidence for incommensurate CDW order was found in the two-dimensional work either.

IV. CONCLUSIONS

The electron-phonon problem (Holstein model) has been examined in the limit of large spatial dimensions. The Holstein model always has CDW solutions in the static limit $\Omega\rightarrow 0$ and always has SC solutions in the instantaneous limit $\Omega\rightarrow\infty$. Away from half-filling, the transition from CDW behavior to SC behavior occurs when $|U|$ is on the order of Ω with SC occurring for the smaller values of $|U|$ and CDW occurring for the larger values of $|U|$. The maximum CDW transition temperature is determined by the electronic energy scale, and is virtually *independent* of the phonon frequency. Its magnitude is on the order of $0.15t^*$ and the maximum occurs at half-filling when the polaron binding energy $|U|$ is on the order of the bandwidth t^*. The maximum SC transition temperature, on the other hand, is very strongly dependent upon the phonon frequency. In the case considered here ($\Omega/t^*=0.5$), the maximum SC transition temperature appears to be an order of magnitude smaller than the maximum CDW transition temperature $T_c(\mathrm{SC})\leq 0.03t^*$ and is expected to be lower for smaller phonon frequencies. The maximum SC transition temperature is always less than the maximum CDW transition temperature.

The effective phonon potential develops a double-well structure as the electron-phonon coupling is increased. The maximum CDW transition temperature occurs when T_c is on the order of the barrier height of the double well. The weak-coupling regime corresponds to the case where the effective phonon potential has a single well and is harmonic ($|U|\ll t^*$) and the strong-coupling regime corresponds to the case where the double-well structure has fully developed and it is difficult to tunnel from one minima to the other via thermal excitations ($|U|\gg t^*$). Accurate approximation techniques must be equally well suited for a single-well and a double-well phonon potential in order to describe the region near the maximum T_c. Neither the conserving Hartree-Fock approximation nor the lowest-order bipolaron theories can achieve this goal.

What is the applicability of these results to finite-dimensional systems and real materials? The infinite-dimensional results appear to agree reasonably well with

previous results in two dimensions[6–9] (when all energy units are rescaled to units of t^*) which shows promise that expansions in powers of $1/d$ may converge rapidly. The electron-phonon problem does seem to show an overwhelming propensity towards CDW behavior (especially at small phonon frequencies), yet most real materials display SC rather than CDW. There are several reasons for this: First, the effective electron-electron interaction strength $|U|$ tends to be small in real materials which implies one is probably on the SC side of the CDW-SC phase boundary. Second, many lattice structures are frustrated. The frustration will reduce the effect of Fermi-surface nesting and reduce the CDW susceptibility accordingly. Frustration is not expected to have as deleterious an effect on SC. Finally, repulsive Coulomb interactions (which have been neglected in this model) will suppress CDW ordering more than SC ordering because the Coulomb interaction is renormalized (logarithmically) due to retardation effects in the SC but is not renormalized for the CDW. It is possible that this last effect can be avoided in a more general model of the Su-Schrieffer-Heeger type[11] where the CDW forms on the bonds and can avoid the on-site Coulomb repulsion.

Further work should include an investigation of how well the conserving fluctuation-exchange[25] approximation works for the Holstein model, a MC simulation of the effects of Coulomb interactions on the electron-phonon system, and an investigation of higher-order strong-coupling expansions.

ACKNOWLEDGMENTS

We would like to acknowledge stimulating discussions with N. Bulut, D. Cox, H. Monien, P. Monthieux, E. Nicol, T. Pruschke, R. Sugar, and S. Trugman. We would especially like to thank J. Hirsch and H.-B. Schüttler for their continued interest in this problem and for many valuable discussions. We also thank H.-B. Schüttler for suggesting our examination of the effective phonon potential [Eq. (32)] and S. Trugman for pointing out the renormalization of the interaction strength in the effective spinless Falicov-Kimball model [Eq. (A3)]. This research was supported at UCSB by the National Science Foundation under Grant Nos. DMR90-02492 and PHY89-04035 and at UC by the National Science Foundation under Grant No. DMR-9107563 and by the Ohio Supercomputer Center.

APPENDIX

The details of the mapping of the Holstein model onto a Falicov-Kimball model in the static limit are given here. In the limit where the phonon frequency approaches zero ($\Omega \to 0$), the phonon coordinate $x(\tau)$ does not change in time and becomes independent of τ. The partition function is then easily determined using the same techniques that were used in solving the spinless Falicov-Kimball model.[15] There are only two differences. First, two species of conduction electrons must be included (one for spin up and one for spin down), and second, the static phonon field can assume a continuum of values rather than the two values allowed in the spinless Falicov-Kimball model. The result is

$$Z=\int_{-\infty}^{\infty} dx\, \exp[-\tfrac{1}{2}\beta M\Omega^2 x^2-\beta(gx-\mu)] \times \prod_{n=-\infty}^{\infty}\left[\frac{i\omega_n+\mu-gx\lambda_n}{i\omega_n}\right]^2, \tag{A1}$$

where the definition

$$G_0^{-1}(\tau-\tau')\equiv\partial_\tau\delta(\tau-\tau')+\lambda(\tau-\tau')$$

is used and λ_n is the Fourier transform of $\lambda(\tau)$. This is the partition function of a Falicov-Kimball model with spin-$\frac{1}{2}$ conduction electrons that interact with $S\to\infty$ localized electrons (that can have a continuous distribution of static configurations). The Falicov-Kimbal model has a constraint, since the chemical potential for the static electrons is not free to vary in Eq. (A1).

In the low-temperature limit, the integral for the partition function can be evaluated by steepest descents. One must recall that the self-consistency condition on the Green's functions produces an implicit x dependence to the time-dependent atomic field $\lambda(\tau)$. The method of steepest descents states that the integral will be dominated by the regions where the exponent is slowly varying. Differentiating the exponent and setting it to zero yields

$$gx=U\left[1+2T\sum_{n=-\infty}^{\infty}\frac{1+g\lambda_n'}{i\omega_n+\mu-gx-\lambda_n}\right]$$
$$=U\left[1-\coth\beta(gx-\mu)+\frac{1}{2}\coth\frac{\beta(gx-\mu)}{2}+2T\sum_{n=-\infty}^{\infty}\frac{1}{i\omega_n+\mu-gx-\lambda_n}\left[\frac{\lambda_n}{i\omega_n+\mu-gx}+g\lambda_n'\right]\right]. \tag{A2}$$

In general, there are three solutions to the steepest descents condition (A2): one near $gx=0$, one near $gx=U$, and one near $gx=2U$. The solution near $gx=U$ is a maximum and can be neglected. If the two solutions near $gx=0$ and $2U$ are well separated ($|U|\to\infty$), then the steepest descents approximation to the integral consists of the sum of the integrands evaluated at these two values of gx; the system looks like a spinless Falicov-Kimball model with the effective interaction set by the difference in energies for the two roots to Eq. (34) ($U_{\rm FK}=gx_2-gx_0$). As the two solutions begin to coalesce towards $gx=U$, the simple steepest descents approximation will fail and one needs to try more elaborate approximation techniques that take into account the in-

terference effects between the two roots.

The particle-hole symmetric case of half-filling corresponds to the choice $\mu=U$. In this case the two roots corresponding to minima in Eq. (A2) are symmetrically displaced [$gx_0=\gamma U$, $gx_2=(2-\gamma)U$] and one finds the renormalized Falicov-Kimball interaction satisfies

$$U_{\rm FK}=2(1-\gamma)U\equiv\frac{U}{\alpha(U)}\ , \tag{A3}$$

and the static electrons are also "half-filled" ($\langle gx_j\rangle=0.5$). Since the mapping that determines the Falicov-Kimball interaction strength is one to one, the renormalization factor α can be viewed as a function of U or of $U_{\rm FK}$. It is simpler numerically to proceed by calculating properties of the spinless Falicov-Kimball model for a given value of $U_{\rm FK}$ and then determine the corresponding value of U for the Holstein model at the end by calculating the renormalization factor α. One finds that in the limit as $U_{\rm FK}\rightarrow-\infty$ that the renormalization factor becomes constant $\alpha\rightarrow0.5$ in a agreement with the strong-coupling expansion of Sec. III. In the limit as $U_{\rm FK}\rightarrow0$, the renormalization factor diverges $\alpha\rightarrow0.578/U_{\rm FK}$. This latter case is unphysical and illustrates the breakdown of the simple steepest descents approximation to the integral in Eq. (A1). The transition temperatures calculated by mapping the Holstein model to the spinless Falicov-Kimball model appear to be accurate for values of U ranging from $-\infty$ to -0.7.

At small values of $|U|$ one can use ordinary conserving Hartree-Fock perturbation theory (in the $\Omega\rightarrow0$ limit) to determine the transition temperature to the commensurate CDW at half-filling. The perturbation theory predicts that the transition temperature has an exponential dependence on $1/U$ in the small $|U|$ limit. The conserving Hartree-Fock calculation appears to be accurate for values of U ranging from 0 to -0.425.

The two approximation techniques (map to spinless Falicov-Kimball model and conserving Hartree-Fock) are joined together in Fig. 1 by a linear interpolation for the transition temperature in the "gap" region $-0.7<U<-0.425$. The resulting curve for the transition temperature to the commensurate CDW (at $X=-1$) in Fig. 1 is probably an accurate approximation to the true transition temperature curve that would be determined by solving the self-consistent problem based upon the full partition function in Eq. (A1).

[1]A. B. Migdal, Zh. Eksp. Teor. Fiz. **34**, 1438 (1958) [Sov. Phys. JETP **7**, 999 (1958)].

[2]G. M. Eliashberg, Zh. Eksp. Teor. Fiz. **38**, 966 (1960) [Sov. Phys. JETP **11**, 696 (1960)].

[3]P. B. Allen and R. C. Dynes, Phys. Rev. B **12**, 905 (1975).

[4]S. Robaszkiewicz, R. Micnas, and K. A. Chao, Phys. Rev. B **23**, 1447 (1981); A. S. Alexandrov, J. Ranninger, and S. Robaszkiewicz, *ibid.* **33**, 4526 (1986); R. Micnas, J. Ranninger, and S. Robaszkiewicz, Rev. Mod. Phys. **62**, 113 (1990).

[5]J. E. Hirsch and E. Fradkin, Phys. Rev. Lett. **49**, 402 (1982); Phys. Rev. B **27**, 4302 (1983).

[6]R. T. Scalettar, N. E. Bickers, and D. J. Scalapino, Phys. Rev. B **40**, 197 (1989).

[7]F. Marsiglio, Phys. Rev. B **42**, 2416 (1990).

[8]R. M. Noack, D. J. Scalapino, and R. T. Scalettar, Phys. Rev. Lett. **66**, 778 (1991).

[9]M. Vekič, R. M. Noack, and S. R. White, Phys. Rev. B **46**, 271 (1992).

[10]T. Holstein, Ann. Phys. **8**, 325 (1959).

[11]W. P. Su, J. R. Schrieffer,and A. J. Heeger, Phys. Rev. B **22**, 2099 (1980).

[12]W. Metzner and D. Vollhardt, Phys. Rev. Lett. **62**, 324 (1989).

[13]H. Schweitzer and G. Czycholl, Z. Phys. B **77**, 327 (1990).

[14]W. Metzner, Phys. Rev. B **43**, 8549 (1991).

[15]U. Brandt and C. Mielsch, Z. Phys. B **75**, 365 (1989); **79**, 295 (1990); **82**, 37 (1991).

[16]F. J. Okhawa, Phys. Rev. B **44**, 6812 (1991); Prog. Theor. Phys. Suppl. **106**, 95 (1991).

[17]A. Georges and G. Kotliar, Phys. Rev. B **45**, 6479 (1992).

[18]M. Jarrell, Phys. Rev. Lett. **69**, 168 (1992).

[19]J. E. Hirsch and R. M. Fye, Phys. Rev. Lett. **56**, 2521 (1986).

[20]M. Jarrell and T. Pruschke, Z. Phys. B **90**, 187 (1993).

[21]M. J. Rozenberg, X. Y. Zhang, and G. Kotliar, Phys. Rev. Lett. **69**, 1236 (1992).

[22]A. Georges and W. Krauth, Phys. Rev. Lett. **69**, 1240 (1992); (unpublished).

[23]V. Zlatić and B. Horvatić, Solid State Commun. **75**, 263 (1990).

[24]E. Müller-Hartmann, Z. Phys. B **74**, 507 (1989); **76**, 211 (1989).

[25]N. E. Bickers and D. J. Scalapino, Ann. Phys. **193**, 206 (1989).

[26]J. Hubbard, Proc. R. Soc. London Ser. A **276**, 238 (1963); **277**, 237 (1964); **281**, 401 (1964); **285**, 542 (1965); **296**, 82 (1967); **82**, 100 (1967).

[27]M. Randeria, J.-M. Duan, and L.-Y. Shieh, Phys. Rev. Lett. **62**, 981 (1989); R. T. Scalettar, E. Y. Loh, J. E. Gubernatis, A. Moreo, S. R. White, D. J. Scalapino, R. L. Sugar, and E. Dagotto, *ibid.* **62**, 1407 (1989); L. Belkhir and M. Randeria, Phys. Rev. B **45**, 5087 (1992).

[28]O. J. Heilmann and E. H. Lieb, Trans. N.Y. Acad. Sci. **33**, 116 (1971); C. N. Yang, Phys. Rev. Lett. **63**, 2144 (1989); M. Pernici, Europhys. Lett. **12**, 75 (1989); S. Zhang, Phys. Rev. Lett. **65**, 120 (1990).

[29]L. M. Falicov and J. C. Kimball, Phys. Rev. Lett. **22**, 997 (1969).

[30]J. K. Freericks, Phys. Rev. B **47**, 9263 (1993).

[31]S. Aubry, G. Abramovici, and J.-L. Raimbault, J. Stat. Phys. **67**, 675 (1992).

[32]P. W. Anderson, J. Phys. Chem. Solids **11**, 26 (1959); G. Bergmann and D. Rainer, Z. Phys. **263**, 445 (1974).

[33]The T_c vs μ^* curves should have a maximum at $\mu^*=0$. The slight increase in T_c for the lowest values of μ^* occurs because of the increased Trotter error in the MC results away from half-filling. We expect that if the MC results were calculated at a smaller value of $\Delta\tau$ and scaled toward $\Delta\tau\rightarrow0$, the transition temperatures would all shift slightly downward (on the order of 5%).

[34]G. Baym and L. P. Kadanoff, Phys. Rev. **124**, 287 (1961); G.

Baym, *ibid.* **127**, 1391 (1962).
[35]The Hartree contribution to the self-energy is a constant that is independent of frequency and can be absorbed into a renormalized chemical potential μ.
[36]C. S. Owen and D. J. Scalapino, Physica **55**, 691 (1971).
[37]J. R. Schrieffer and P. A. Wolff, Phys. Rev. **149**, 491 (1966).
[38]A. B. Harris and R. V. Lange, Phys. Rev. **157**, 295 (1967).
[39]G. Beni, P. Pincus, and J. Kanamori, Phys. Rev. B **10**, 1896 (1974).
[40]J. Mustre de Leon, I. Bastić, A. R. Bishop, S. D. Conradson, and S. A. Trugman, Phys. Rev. Lett. **68**, 3236 (1992); J. Zhong and H.-B. Schüttler, *ibid.* **69**, 1600 (1992).
[41]C. C. Yu and P. W. Anderson, Phys. Rev. B **29**, 6165 (1984).